Acta Oncologica 29 (1990) Fasc. 4

FROM THE DEPARTMENT OF RADIATION PHYSICS, THE KAROLINSKA INSTITUTE AND THE UNIVERSITY OF STOCKHOLM, STOCKHOLM, SWEDEN.

PHOTON BEAM ENERGY DEPOSITION KERNELS FOR INVERSE RADIOTHERAPY PLANNING

A. EKLÖF, A. AHNESJÖ and A. BRAHME

Abstract

A method for calculating energy deposition kernels for planar convergent isotropic irradiations of a point target has been developed. A geometric overlap algorithm is applied to pencil beam energy deposition kernels calculated by convolution of Monte Carlo generated point spread functions with the energy released by a point monodirectional photon beam. The geometric overlap interpolation technique is energy conservative and hence, for dosimetric purposes, more precise than interpolations based on smoothing techniques. Furthermore, due to the integration processes involved, most of the statistical noise in the original Monte Carlo data is eliminated. The resulting kernels have a precision and noise level corresponding to 10^9–10^{10} Monte Carlo simulated photons. The kernels are useful for inverse conformation therapy planning, and for dose planning with small target volumes.

Key words: Photon therapy planning, energy deposition kernels, photon pencil beams, rotated pencil beams, inverse radiotherapy planning.

Photon beam dose planning is currently in a state of rapid development with several new and powerful mathematical methods under implementation for clinical use. For example, accurate analytical, experimental and Monte Carlo generated energy deposition kernels (1–6) are taken into use to describe the energy transport by secondary particles released by the primary photons. Convolution methods for therapy planning, making use of such kernels, will allow considerably increased accuracy in 3-dimensional photon scatter integration and consideration of the significant secondary electron range in high energy photon beams. Furthermore, inverse radiation therapy planning (IRP) techniques allow deterministic calculation of the optimal set of incident beams from the desired dose distribution in the target volume (7, 8). IRP thus allows a substantial improvement in controlling the dose delivery through an optimization of the incoming beam shapes. In comparison to conventional forward therapy planning, IRP is a reverse process, since the desired dose distribution in the target volume and specified maximal doses to organs at risk are deterministically used to derive the optimal profiles of the required incident beams. The only complication is that the required fluence distributions of the incident beams will most often be non-uniform in contrast to conventional treatment planning where uniform or wedge shaped beams are generally employed. It has recently been shown that the use of such non-uniform incident beams have the potential to considerably lower the delivered dose to normal tissues, particularly near concave sections of the target volume (7).

In a similar way as convolution based photon therapy planning uses point spread functions (PSFs) as energy deposition kernels, IRP requires elementary energy deposition kernels of the incident photon beams. For a plane parallel photon beam the natural kernel is that generated by a narrow pencil photon beam. Such photon pencil beams were calculated directly with Monte Carlo methods by Schoknecht (9) for 1.25 MeV and Mohan & Chui (10) for a number of energies. Such kernels can be accurately calculated from cylindrically symmetric point spread functions, cf. eq. (2). In the present paper we use such pencil beam kernels to calculate the energy deposition kernel due to planar convergent irradiations of a point target. These 'rotated pencil beams' are the elementary convolution kernels for generalized conformation therapy, and have previously been approximated using analytical methods (7). The term 'rotated pencil beam', which will be used throughout the paper for this irradiation geometry, applies to the isotropic incidence in a plane on

Accepted for publication 22 March 1989.

a point target by photon pencil beams, as illustrated in Fig. 1. In a forthcoming work these kernels will be applied on various complex target volumes to determine the optimum dose distribution and photon energy.

Theory

Point spread functions

A set of point spread functions for monoenergetic photons in water has previously been calculated (5). This set has been extended up to 50 MeV (11), using the same Monte Carlo code (12). In the Monte Carlo calculation, monoenergetic photons directed along the central axis of a cylindrical water phantom are forced to interact at a selected depth z_0 on the central axis. The energy deposition around this interaction point is scored within a cylindrical volume of length 51.2 cm and diameter 51.1 cm.

The scoring volume is divided into cylindrical voxels, of radial and longitudinal increments, Δr_{cyl} and Δz_{cyl}, both of size 1 mm. The voxel (m, n) covers the longitudinal range $z_{n-1}<z<z_n$, where $z_n=n\Delta z_{cyl}-z_0$, and the radial range $r_{m-1}<r<r_m$, where $r_m=(m-0.5)\Delta r_{cyl}$. For m=1 the radial range is $0<r<\Delta r_{cyl}/2$. For initial photon energies up to 10 MeV, z_0 is set to 25.65 cm, which is close to the center of the scoring volume. For higher photon energies a smaller interaction depth is selected in order to score the major part of the bremsstrahlung and compton scattered photons, which are mainly forward directed at these energies. The phantom geometry is shown in Fig. 2.

The fractional mean energy imparted $H_{m,n}$ in voxel (m, n) is equal to the integral of the continuous PSF, $h(\vec{r})=h(r,z)$, over the volume of the voxel:

$$H_{m,n}=\int_{z_{n-1}}^{z_n}\int_{r_{m-1}}^{r_m} h(r,z)\,2\pi r\,dr\,dz \qquad (1)$$

The integration is implicitly done by means of Monte Carlo simulation.

Pencil beams

The pencil beam kernel $p(\vec{r})$ is calculated from the PSF through the convolution:

$$p(r,z)=\int h(r,z-z')\,\mu e^{-\mu z'}\,dz' \qquad (2)$$

where μ is the linear attenuation coefficient of the impinging monoenergetic photons and z' is the depth of the primary interaction. In this work, a finite phantom thickness of 25 cm has been used when calculating the pencil beam kernels, so a finite integral from z=0 to z=25 cm has been calculated. In practice the discrete representation given by eq. (1) is used, and eq. (2) is replaced by a sum:

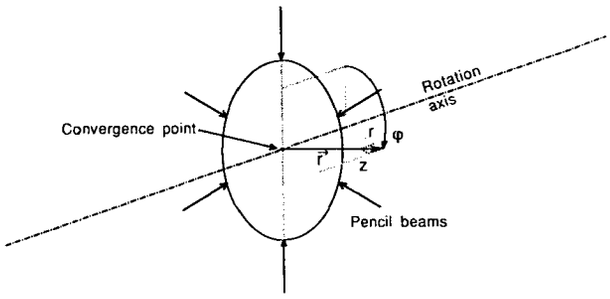

Fig. 1. Illustration of the term 'rotated pencil beam'. The notations used in eq. (4) are included.

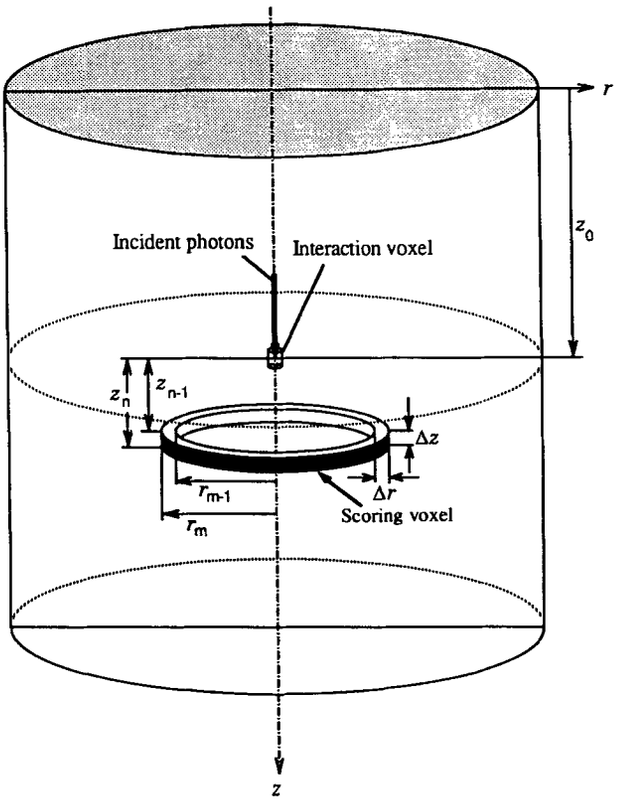

Fig. 2. The geometry of the Monte Carlo phantom, with the interaction voxel and one ringshaped scoring voxel indicated.

$$P^{cyl}_{m,n}=\sum_{v=1}^{n_z} H_{m,n-v+1}\,\mu e^{-\mu z}\,\Delta z_{cyl} \qquad (3)$$

where v is the longitudinal index of the voxel of the primary interaction, n_z is the number of longitudinal bins, and $z=(v-0.5)\Delta z_{cyl}$ is the depth of the center of the interaction voxel. The mean energy imparted in each voxel is stored in the same cylindrical geometry as of the

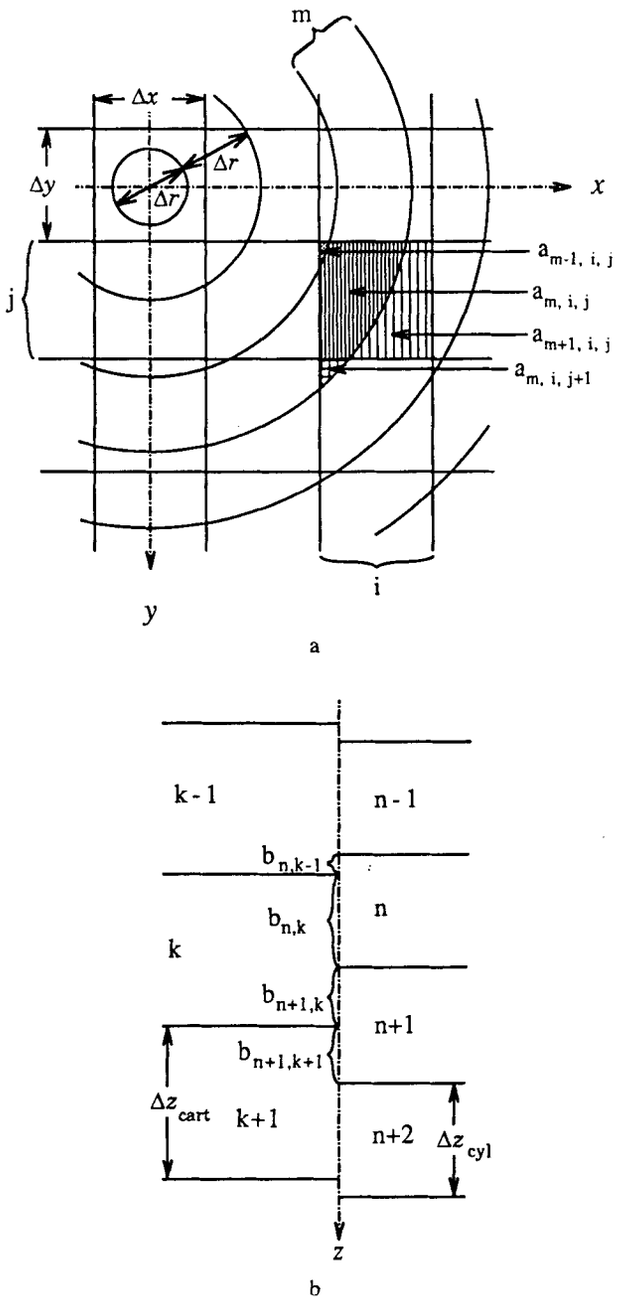

Fig. 3. Illustration of the overlap indices of a) the area overlap between cylindrical and cartesian pixels and b) the depth overlap of the longitudinal bins if the cylindrical axis and the corresponding cartesian bins.

PSF:s, but with n_z(=250) longitudinal bins, and the origin at the phantom surface.

Rotated pencil beams

The energy depositions caused by a rotated pencil beam, centered at the axis of a cylindrical phantom, can be calculated from the pencil beam kernel through a closed line integral (cf. Fig. 1):

$$c(r,z) = \oint p(r,z)\,\delta\varphi/2\pi \qquad (4)$$

where r and z are the radial and longitudinal distances respectively, measured from the convergence point in the phantom and is the incidence angle of the pencil beam.

The most straightforward way to numerically calculate the integral in eq. (4) would be to sample the kernel at equidistant points along circles of radius r. However, there are severe problems with this method, due to high gradients in the radial direction near the axis. At any depth z, the kernel p(r, z) has a singularity at r=0, and it is generally not possible to accurately fit a simple, well-behaved function in the proximity of the central axis of the pencil beam. Analytical fits may be used for accelerator spectra, but due to the cylindrical symmetry, integration over a cartesian voxel is very complex. Furthermore, analytical fits do not preserve energy locally. In order to conserve energy and reduce computation time a geometric overlap technique has been developed.

Method

The area overlap technique

Instead of summing samples of the energy deposition kernel along circles, as implied by eq. (4), we do the integration by a two-step transformation. First, the pencil beam energy deposition kernel is rebinned from cylindrical voxels to a 3-dimensional cartesian coordinate system, and then to a second cylindrical coordinate system, with its z axis defined as the rotation axis in Fig. 1, that is, perpendicular to the plane of the incident pencil beams.

The mean energy imparted in each cartesian voxel is calculated by weighing the mean energy imparted in the original cylindrical pencil beam voxels intersecting the cartesian voxel, using the intersected volumes as weighing factors. Since the origin and the z-axis of the two coordinate systems are defined to coincide, the calculation of weighing factors can be divided into two parts: the length overlap in depth, and the area overlap in a plane perpendicular to the incoming beam. These overlaps are illustrated in Fig. 3.

The fractional mean energy imparted in a cartesian voxel, $P^{cart}_{i,j,k}$, can be expressed as the sum of the contributions from all the cylindrical voxels intersecting it:

$$P^{cart}_{i,j,k} = \sum_{m=1}^{n_r} a_{m,i,j} \sum_{n=1}^{n_z} b_{n,k}\, P^{cyl}_{m,n}/V^{cyl}_{m} \qquad (5)$$

where $a_{m,i,j}$ is the area overlap, or common base area of the radial bin m and the cartesian pixel (i,j), $b_{n,k}$ is the length overlap between the longitudinal bins n and k, and V^{cyl}_{m} is the volume of the cylindrical voxels.

For m=1, $V^{cyl}_{m}=\pi\Delta r_{cyl}{}^2\Delta z_{cyl}/4$, else (m>1), $V^{cyl}_{m}=2\pi(m-1)\,\Delta r_{cyl}{}^2\Delta z_{cyl}$. When there is no overlap $a_{m,i,j}=0$, or

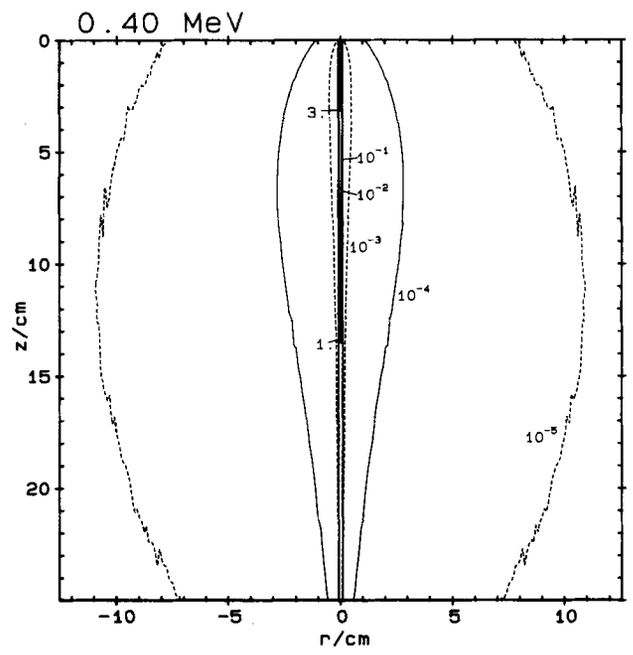

a

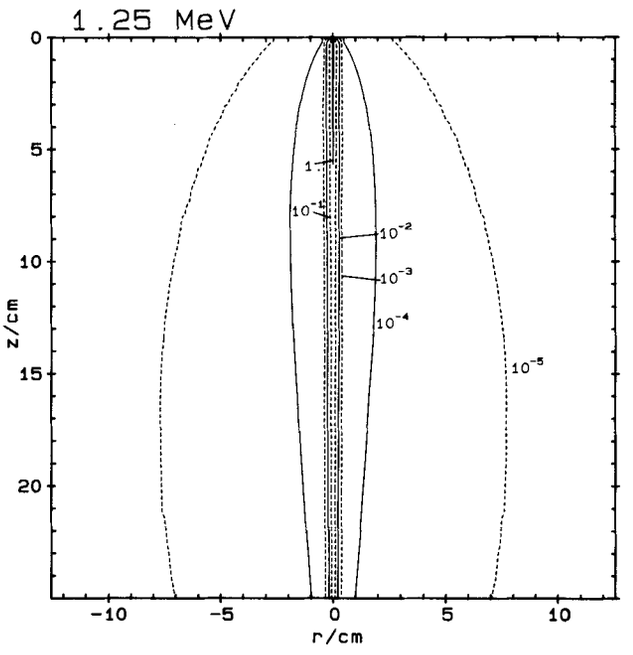

b

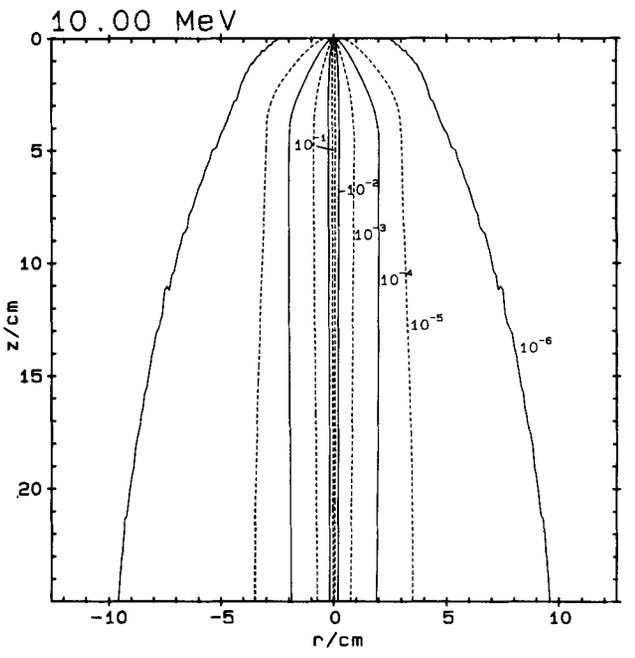

c

Fig. 4. Isolevels of photon pencil beam kernels $\vec{p}(r)$, shown as fractional energy imparted per unit volume (cm^{-3}), in a 25 cm water slab for monoenergetic incident photons of the energies a) 0.4 MeV, b) 1.25 MeV and c) 10 MeV. The maximum values are 4.12, 1.39 and 0.226 cm^{-3} respectively.

$b_{n,k}=0$ respectively. If we set $\Delta z_{cart}=\Delta z_{cyl}$, all $b_{n,k}$ will be identical and equal to z_{cart}, which reduces eq. (5) to:

$$P^{cart}_{i,j,k} = \sum_{m=1}^{n_r} a_{m,i,j}\,\Delta z_{cart}\,P^{cyl}_{m,k}/V^{cyl}_{m} \qquad (6)$$

Since $a_{m,i,j}$ will be independent of depth, it is possible to precalculate all the necessary area overlaps $a_{m,i,j}$, and thus reduce the computation time considerably. Given the energy deposition in the cartesian coordinate system, the second step is performed by rebinning the energy deposition to a second cylindrical coordinate system with its central axis defined as the rotation axis. This coordinate system is defined with its origin at the point of convergence, and its central axis coinciding with the y-axis of the cartesian coordinate system, that is, perpendicular to the direction of the pencil beam. The fractional mean energy imparted in a voxel of this system can be expressed:

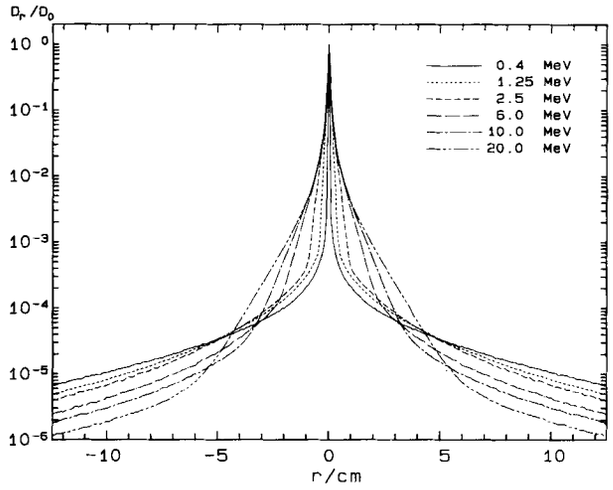

Fig. 5. Normalized pencil beam profiles at a depth of 12.5 cm for 6 incident photon energies in a 25 cm water slab.

Table 1

Fractional energy deposition and fractional mean energy imparted per unit volume at maximum for monoenergetic photon pencil beams in a 25 cm water slab at a voxel size of 1 mm

Initial photon energy (MeV)	Fraction of initial energy deposited in the phantom	Fractional mean energy imparted per unit volume at maximum (cm^{-3})
0.4	0.6652	4.126
1.25	0.5845	1.389
2.5	0.4921	0.633
6.0	0.3745	0.3025
10.0	0.3223	0.2264
20.0	0.2720	0.1852

Table 2

Fractional energy deposition and fractional mean energy imparted per unit volume at maximum for rotated monoenergetic photon pencil beams in a cylindrical water phantom of 25 cm diameter at a voxel size of 1 mm

Initial photon energy (MeV)	Fraction of initial energy deposited in the phantom	Fractional mean energy imparted per unit volume at maximum (cm^{-3})
0.4	0.571	0.8759
1.25	0.538	0.5294
2.5	0.471	0.3126
6.0	0.366	0.1841
10.0	0.317	0.1480
20.0	0.269	0.1278

$$C_{m,n} = \int_{z_{n-1}}^{z_n} \int_{r_{m-1}}^{r_m} p(r,z)\, 2\pi r\, dr_{rot}\, dz_{rot} \qquad (7)$$

Eq. (7), where the subscript rot indicates the rotated pencil beam geometry, is analogous to eq. (1), except that $r_m=(m-0.5)\Delta r_{rot}$ ($r_0=0$) and $z_n=(n-0.5)\Delta z_{rot}$ ($z_0=0$), representing the radial and longitudinal distance from the point of convergence, in phantom coordinates. Due to the discrete representation $P^{cart}_{i,j,k}$ of the pencil beam kernel p(r, z) this integration can be done by the same area overlapping algorithm that was used to obtain $P^{cart}_{i,j,k}$:

$$C_{m,n} = \sum_{i=1}^{n_x} \sum_{k=1}^{n_z} a_{m,i,k} \sum_{j=1}^{n_y} b_{n,j} P^{cart}_{i,j,k} / \Delta x \Delta y \Delta z_{cart} \qquad (8)$$

where $\Delta x\Delta y\Delta z_{cart}$ is the volume of the cartesian voxel, and $a_{m,i,k}$ and $b_{n,j}$ have a meaning similar to $a_{m,i,j}$ and $b_{n,k}$ in eq. (5), but here the cartesian y and z coordinates are shifted. If $\Delta z_{rot}=\Delta y$, all $b_{n,k}=\Delta y$ and eq. (8) reduces to:

$$C_{m,n} = \sum_{i=1}^{n_x} \sum_{k=1}^{n_z} a_{m,i,k} P^{cart}_{i,n,k} / \Delta x \Delta z_{cart} \qquad (9)$$

which is analogous to eq. (6).

Results

Pencil beams

Pencil beam kernels have been calculated for the following primary photon energies: 0.4, 1.25, 2.5, 6.0, 10.0 and 20.0 MeV. In Fig. 4 the pencil beam energy depositions are shown as isoenergy deposition levels (cm^{-3}) for 0.4, 1.25 and 10.0 MeV, analogous to Fig. 2 of (5). Radial beam profiles at 12.5 cm depth, normalized to the mean energy imparted per unit volume at the central axis, are shown in Fig. 5. In theory, the pencil beam profiles should have a singularity at the origin, but this is largely lost due to the discretization. The energy fractions deposited in the phantom and the fractional mean energy imparted per unit volume at maximum are shown in Table 1.

The shape of the isolevels is very smooth, compared to directly Monte Carlo calculated pencil beams, due to the convolution of 250 PSFs, each calculated with 500000 photons. From a statistical point of view, this makes the energy deposition comparable to that of a single Monte Carlo run using over 10^8 photons. When the pencil beam kernels are used for absorbed dose calculations, the absorbed dose will be overestimated close to surfaces since the perturbation of scattered photons beyond the phantom boundaries is not taken into account in the Monte Carlo simulations. In general, these effects will however be negligible, except for very large fields at low energies, where the contribution from scattered photons is significant (13).

Rotated pencil beams

Using the described overlap technique, energy deposition kernels for rotated pencil beams have been calculated. For each photon energy kernels were calculated for Δr_{rot} and Δz_{rot} equal to 1, 2, 3 and 4 mm. In each case Δx and Δy were equal to Δr_{rot} and Δz_{rot}. Δz_{cart} was equal to

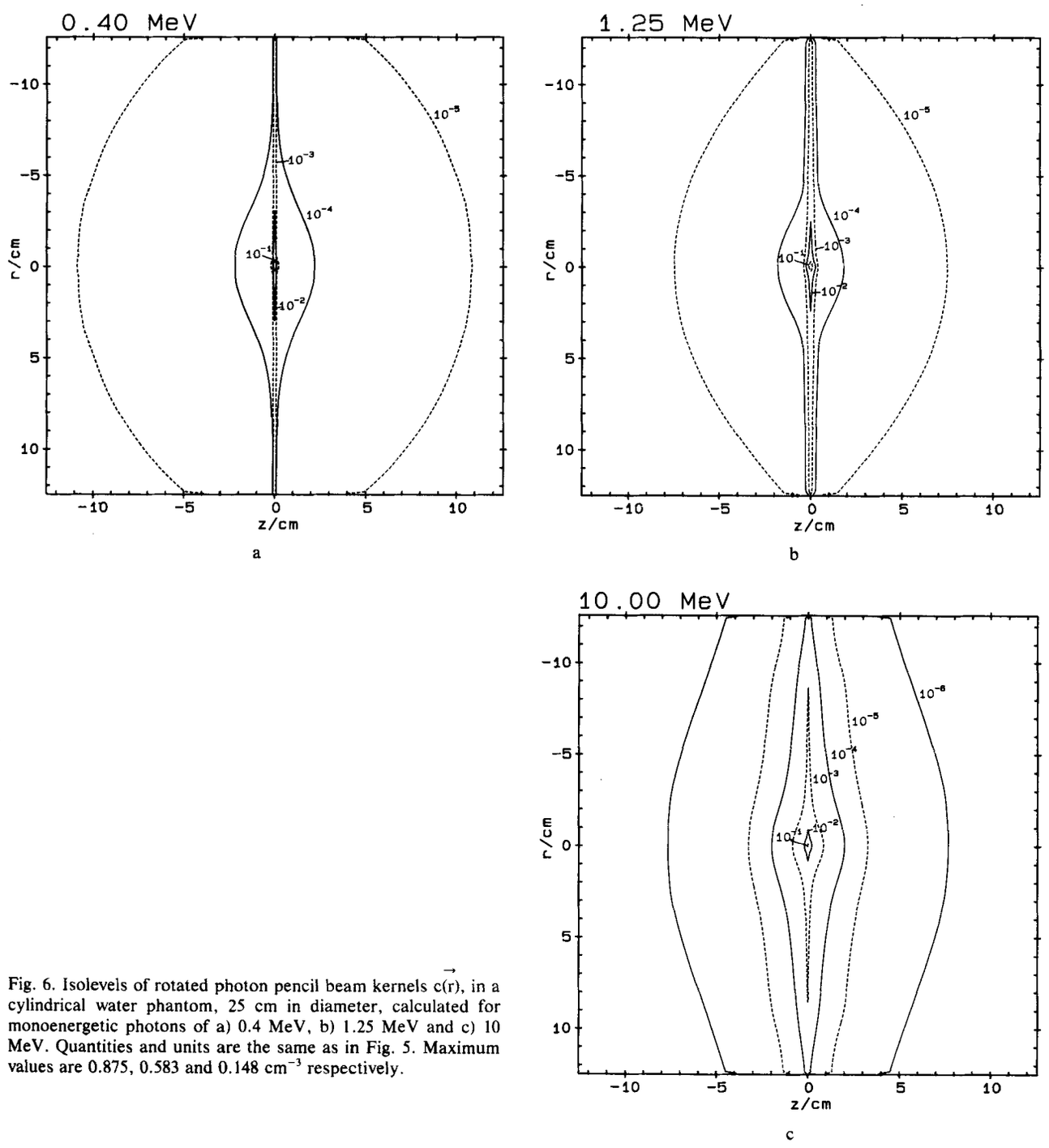

Fig. 6. Isolevels of rotated photon pencil beam kernels $\vec{c}(r)$, in a cylindrical water phantom, 25 cm in diameter, calculated for monoenergetic photons of a) 0.4 MeV, b) 1.25 MeV and c) 10 MeV. Quantities and units are the same as in Fig. 5. Maximum values are 0.875, 0.583 and 0.148 cm^{-3} respectively.

Δz_{cyl} (cf. eq. 6). The fractional energy deposited in the phantom and the fractional mean energy imparted per unit volume in the central voxel, i.e. at the point of convergence, for the 1 mm voxel size are shown in Table 2.

Isoenergy deposition levels (cm^{-3}) from rotated pencil beams, calculated using 1 mm voxels, are shown in Fig. 6. Radial and longitudinal profiles of the energy depositions are plotted in Fig. 7. The profiles have been normalized to the mean energy imparted per unit volume in the central voxel. As can be seen in Fig. 7b, the profiles along the axis of rotation are very similar to the radial profiles of the pencil beams shown in Fig. 5. This is expected, since the energy deposition on the rotation axis is independent of the direction of the pencil beam.

Two important energy dependent effects can be seen in the figures:

For the lowest photon energies, a considerable part of the energy is deposited close to the plane of rotation. This

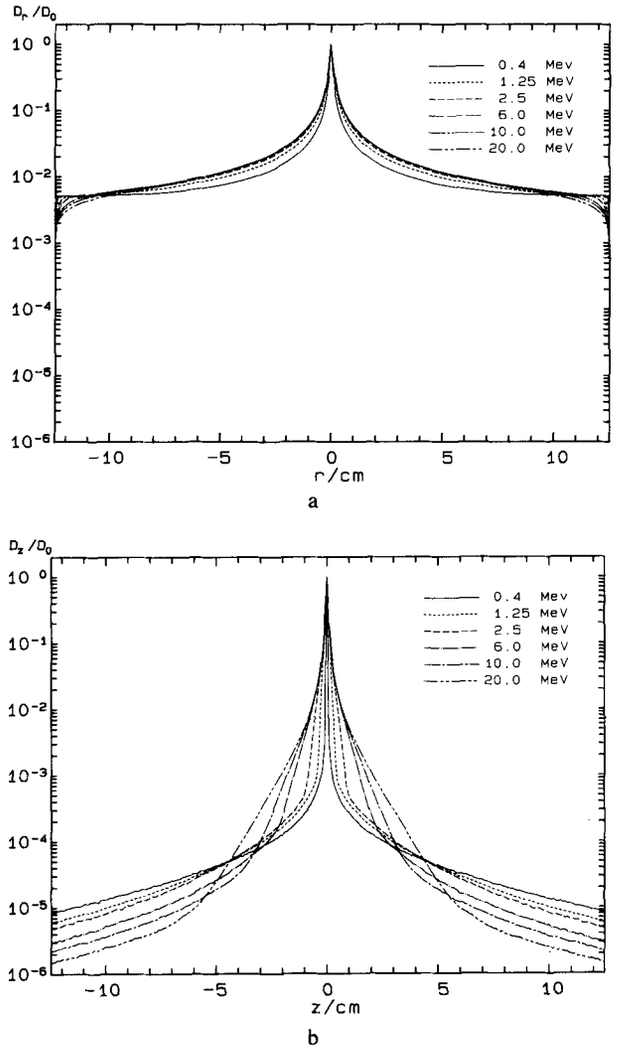

Fig. 7. Normalized radial and longitudinal profiles from rotated pencil beams in a cylindrical water phantom, 25 cm in diameter: a) radial profiles in the plane of rotation and b) longitudinal profiles on the axis of rotation.

is due to the short range of the electrons released by primary photon interaction. As energy increases, so does the range of the electrons, and thus the energy is deposited at larger distances.

At large distances from the plane of rotation an opposite effect can be seen: at low photon energies the energy deposition from secondary photons is about one order of magnitude higher than at high energies. When the incident photon energy increases, the energy deposition at a given distance, outside the electron range, gradually decreases. This is partly due to the fact that the mean scattering angle in Compton interaction, as well as the mean emission angle of bremsstrahlung photons, decrease significantly with increasing energies (forward scattering). Another contributing factor is that the absorbed energy fraction in the primary interaction, E_{abs}/E, increases with energy.

Table 3a

Fractional energy deposition in a 16 cm cube within the cylindrical phantom at different selected voxel sizes for storage of the rotated pencil beam kernels

	Voxel size			
Energy/MeV	1 mm	2 mm	3 mm	4 mm
0.4	0.35364	0.35361	0.35356	0.35349
1.25	0.36740	0.36737	0.36733	0.36727
2.5	0.33172	0.33170	0.33166	0.33160
6.0	0.27032	0.27030	0.27027	0.27022
10.0	0.24160	0.24157	0.24154	0.24149
20.0	0.21151	0.21149	0.21146	0.21142

Table 3b

Fractional energy imparted per unit volume in a 0.5 cm cubic voxel centered at the point of convergence at different selected voxel sizes for storage of the rotated pencil beam kernels (cm^{-3})

	Voxel size			
Energy/MeV	1 mm	2 mm	3 mm	4 mm
0.4	0.005020	0.004718	0.004003	0.003828
1.25	0.007003	0.006154	0.005344	0.005337
2.5	0.005193	0.004651	0.004032	0.003995
6.0	0.003149	0.002840	0.002486	0.002462
10.0	0.002479	0.002239	0.001962	0.001943
20.0	0.001957	0.001774	0.001551	0.001534

To check that energy is conserved during the coordinate transformations, eq. (5) was used for rebinning each of the rotated pencil beam kernels to a cartesian geometry. The voxel size was defined 0.5 cm cubic. The energy deposited in a 16×16×16 cm cube was calculated, as well as the mean energy imparted in the central voxel. The differences in total energy deposition in the cube were found to be negligible (<0.05%) for energy deposition from the same initial photon energy (Table 3a). The differences in mean energy imparted in the central voxel were significant, up to 25% (Table 3b). This is however expected from the high dose gradient effects discussed below.

Discussion

The method described in this work is well suited for calculating the energy deposition kernels from convergent point irradiation, which is an elementary energy deposition kernel for generalized conformation therapy planning (7). The area overlap technique used here has several advantages over interpolation techniques based on smoothing functions, such as spline interpolation:

First, it is strictly energy conservative, in the sense that the total energy deposited in the phantom is preserved (except for energy cut off at the phantom boundaries), even though it is slightly redistributed spatially.

Second, it is much less time-consuming (minutes rather than hours of CPU time on a VAX 8200), than spline interpolation techniques.

The statistical noise from the Monte Carlo calculated point spread kernels is reduced to negligible levels. The noise level is estimated to be comparable to a Monte Carlo run of 10^9–10^{10} photons or more, depending on the number of pencil beam voxels contributing to each voxel value of the resulting kernel. The number of contributing voxels, in its turn, is roughly proportional to the voxel size in the resulting kernel and the distance from the rotation axis.

A minor drawback of the method described here is that due to high dose gradients, the deposited energy will be slightly redistributed in the phantom. This causes a smoothing (of the energy deposition), expected to increase with voxel size, which is in agreement with our results (Table 3b). However, the displacement is generally smaller than the size of the voxels, which makes the problem negligible in ordinary treatment planning.

In a proceeding work, we will use these energy deposition kernels to derive optimized dose distributions for different target volumes.

ACKNOWLEDGEMENT

The authors are indebted to Pedro Andreo for numerous valuable discussions and suggestions.

Request for reprints: A. Eklöf, Department of Radiation Physics, P.O. Box 60211, S-104 01 Stockholm, Sweden.

REFERENCES

1. Ahnesjö, A, Mackie R. Analytical description of Monte Carlo generated photon dose convolution kernels. Proc. 9th Int. Conf. on Computers in Radiation Therapy. Bruinvis IAD, van dir Gressen PH, van Kleffens HJ, eds. Amsterdam, Holland: Elsevier, 1987; 197–200.
2. Boyer A, Mok E. A photon dose distribution model employing convolution calculations. Med Phys 1985; 12: 169–77.
3. Chui C, Mohan R. Extraction of pencil beam kernels by the deconvolution method. Med Phys 1988; 15: 138–44.
4. Ahnesjö A. Collapsed cone convolution of radiant energy for photon dose calculation in heterogeneous media. Med Phys 1989; 16: 577–92.
5. Ahnesjö A, Andreo P, Brahme A. Calculation and application of point spread functions for treatment planning with high energy photon beams. Acta Oncol 1987; 26: 49–56.
6. Mackie TR, Bielajew AL, Rogers DWO, Battista JJ. Generation of photon energy deposition kernels using the EGS Monte Carlo code. Phys Med Biol 1988; 33: 1–20.
7. Brahme A. Optimizations of conformation and generalized moving beam radiation therapy techniques. Radiother Oncol 1988; 12: 129–40.
8. Lind B, Brahme A. Optimization of radiation therapy dose distributions using scanned electron and photon beams and multileaf collimators. Proc. 9th Int. Conf. on Computers in Radiation Therapy, Bruinvis IAD, van der Giessen PH, van Kleffens HJ, eds. Amsterdam: Elsevier, North Holland, 1987: 235–9.
9. Schoknecht G. Die Berechnung von Strahlenfeldern durch Separierung von Primär- und Sekundärstrahlung. IV. Berechnung von Streuverteilungen für parallele Photonenstrahlenfelder. Strahlenterapie 1971; 141: 326–31.
10. Mohan R, Chui C. Use of fast Fourier transforms in calculating dose distributions for irregularly shaped fields for three-dimensional treatment planning. Med Phys 1987; 14: 70–7.
11. Ahnesjö A, Andreo P. Determination of bremsstrahlung spectra and electron contamination from therapeutic photon beam depth dose data. Phys Med Biol 1989; 34: 1451–64.
12. Andreo P. Monte Carlo simulation of electron transport in water. Absorbed dose and fluence distributions. Report FANZ/80/3, Dept of Nuclear Physics, University of Zaragoza, Spain 1980.
13. Ahnesjö A. Invariance of convolution kernels applied to dose calculations for photon beams. Proc. 9th Int. Conf. on Computers in Radiation Therapy, Bruinvis IAD, van der Giessen PH, van Kleffens HJ, eds. Amsterdam: Elsevier, North Holland, 1987: 99–102.